The Journal of Experimental Biology 213, 1217-1225

doi:10.1242/jeb.034660

A wake-based correlate of swimming performance and foraging behavior in seven co-occurring jellyfish species

J. O. Dabiri[1,*], S. P. Colin[2], K. Katija[1] and J. H. Costello[3]

[1]Graduate Aeronautical Laboratories and Bioengineering, California Institute of Technology, Pasadena, CA 91125, USA, [2]Environmental Science and Marine Biology, Roger Williams University, Bristol, RI 02809, USA and [3]Biology, Providence College, Providence, RI 02918, USA

*Author for correspondence (jodabiri@caltech.edu)

Accepted 15 December 2009

SUMMARY

It is generally accepted that animal–fluid interactions have shaped the evolution of animals that swim and fly. However, the functional ecological advantages associated with those adaptations are currently difficult to predict on the basis of measurements of the animal–fluid interactions. We report the identification of a robust, fluid dynamic correlate of distinct ecological functions in seven jellyfish species that represent a broad range of morphologies and foraging modes. Since the comparative study is based on properties of the vortex wake – specifically, a fluid dynamical concept called optimal vortex formation – and not on details of animal morphology or phylogeny, we propose that higher organisms can also be understood in terms of these fluid dynamic organizing principles. This enables a quantitative, physically based understanding of how alterations in the fluid dynamics of aquatic and aerial animals throughout their evolution can result in distinct ecological functions.

Supplementary material available online at http://jeb.biologists.org/cgi/content/full/213/8/1217/DC1

Key words: jellyfish, swimming, vortex formation, wakes.

INTRODUCTION

Animal–fluid interactions have been hypothesized as a principal selective pressure on the evolution of aquatic and aerial animals (e.g. Thompson, 1942; Lighthill, 1975; Vogel, 1994; Fish and Lauder, 2006). However, attempts to discover the fluid dynamic mechanisms that dictate the fitness of animals have been limited by an inability to measure the fluid interactions of freely moving animals (i.e. in the absence of tethers or artificial water or wind currents) in comparative studies of multiple species with known evolutionary histories. Where fluid dynamics have been successfully quantified in parallel with biological function (e.g. cardiovascular flows), broad fluid dynamic organizing principles have been achieved [e.g. Murray's Law (Murray, 1926)]. In this paper, we seek similar success in the context of biological propulsion.

Jellyfish provide a unique perspective on the evolution of propulsion by aquatic animals. Medusae were the earliest metazoans to achieve muscle-powered locomotion in water and they did so with a remarkably restricted array of cell types for body construction (Bonner, 1965; Valentine et al., 1994; Valentine, 2004). Their radially symmetrical body plans makes their wake structures more amenable to empirical quantification using methods such as digital particle image velocimetry (DPIV) (Willert and Gharib, 1992). We selected seven species of hydrozoan jellyfish for this comparative study, representing a broad range of morphologies and swimming behaviors: *Aequorea victoria*, *Leuckartiara* sp., *Melicertum octocostatum*, *Mitrocoma cellularia*, *Neoturris* sp., *Phialidium gregarium* and *Sarsia* sp. (Fig. 1). The ecology of these species has been studied since the early work of Kramp (e.g. Kramp, 1959), and their phylogenetic relationships are relatively well known (Bouillon and Boero, 2000; Marques and Collins, 2004; Collins et al., 2006). However, their animal–fluid interactions have been primarily described in qualitative terms (e.g. Colin and Costello, 2002; Dabiri et al., 2005).

We used digital particle image velocimetry (DPIV) measurements to calculate wake kinetic energy, drag and swimming speed of the seven co-occurring species of free-swimming jellyfish. Using this new data, we demonstrate that the swimming and foraging behavior are related to a robust fluid dynamic threshold between two distinct configurations of the wake vortex rings. Specifically, as the wake vortices grow during the formation process, which occurs during the contraction phase of medusan swimming, the vortices can approach a physical limit on their size that occurs due to the energetic requirements of vortex ring formation (Benjamin, 1976). In some medusae this limit is not reached and they form a single vortex ring in their wake. In others, the vortex ring reaches this size limit and can no longer entrain additional fluid, instead forming a trailing jet of fluid behind the vortex ring.

Wake vortices formed near the transition between the two wake vortex configurations (i.e. isolated vortex ring versus vortex ring with trailing jet) maximize the fluid dynamic thrust generated for a given energy input (Krueger and Gharib, 2003). Hence, the formation of these wakes is known in the fluid dynamics literature as optimal vortex formation (e.g. Gharib et al., 1998; Mohseni et al., 2001; Linden and Turner, 2001; Krueger and Gharib, 2003; Dabiri, 2009). By comparing the observed wake structures created by each jellyfish species with the optimal vortex configuration, we are able to predict their relative swimming efficiencies and proficiencies and to integrate these with medusan ecological roles.

Given the generality of the optimal vortex formation concept (Benjamin, 1976) and in light of the prevalence of vortex formation in swimming and flying animals (e.g. Lighthill, 1973; Raynor, 1979), we propose that this comparative study of these basal metazoans might be reproducible in higher animals provided that appropriate

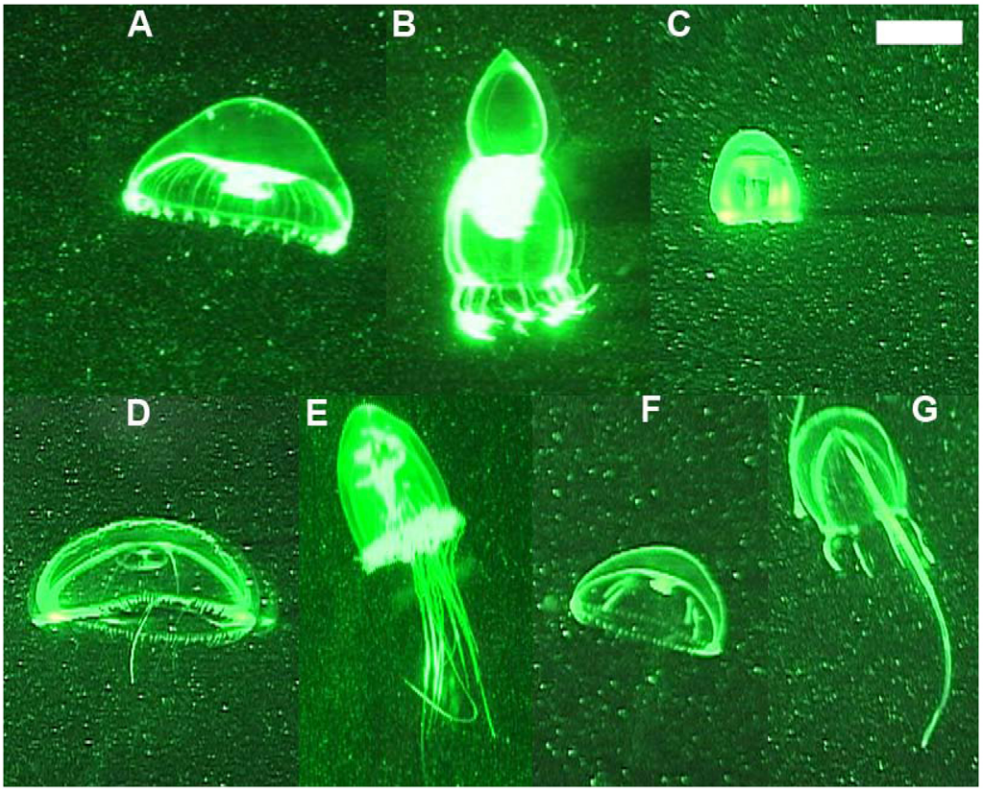

Fig. 1. Hydrozoan jellyfish as observed in digital particle image velocimetry (DPIV) experiments. (A) *Aequorea*, (B) *Leuckartiara*, (C) *Melicertum*, (D) *Mitrocoma*, (E) *Neoturris*, (F) *Phialidium*, (G) *Sarsia* sp. 532-nm (green) light from the source laser sheet is scattered by the animal tissue and by natural particulate in the seawater. Scale bar, 1 cm.

measurements of the animal–fluid interactions are available. Our objective for the present study is to establish a template for those future investigations.

MATERIALS AND METHODS

Animal collection

Individual *Aequorea victoria* (Murbach and Shearer 1902), *Leuckartiara* sp., *Melicertum octocostatum* (Sars 1835), *Mitrocoma cellularia* (Agassiz 1865), *Neoturris* sp., *Phialidium gregarium* [a synonym for the less commonly known but currently accepted *Clytia gregaria* (Agassiz 1862)] and *Sarsia* sp. medusae were hand collected in jars from a dock at the Friday Harbor Laboratories on San Juan Island, WA, USA in May 2007. For simplicity and because there were no congeners present for any of these species, we have referred to the species by their genus name in the text. Specimens were maintained in laboratory vessels containing unfiltered seawater at room temperature (approximately 20°C) and were video recorded within 24 h of collection.

Velocity and vorticity field measurement

Individuals were video recorded while freely swimming in tanks significantly larger than their body size (minimum 10-liter vessels for animals with a 1–3 cm typical bell diameter), to avoid wall effects or other artifacts of the laboratory environment (Vogel, 1994). Velocity fields were measured using digital particle image velocimetry (DPIV) (Willert and Gharib, 1992). Animals were monitored for sequences of swimming initiated symmetrically in the plane of a 1-mm thick vertical sheet of light produced by a 250 mW, 532 nm diode-pumped solid-state laser (Wicked Lasers, Quarry Bay, Hong Kong, PR China). The condition of symmetry in the plane of the laser sheet was determined visually by ensuring that the laser bisected the animal body. The laser sheet illuminated natural particulates in the seawater (typically 10–100 μm), and the particle motion induced by the animal swimming was recorded at 30 Hz onto a digital video (DV) tape *via* a 720×480-pixel CCD array (Sony HDR-FDX1, Sony Electronics Inc., Fort Myers, FL, USA). Consecutive images of each video were interrogated with a custom DPIV algorithm (courtesy of M. Gharib, California Institute of Technology), using an interrogation window size of 32×32 pixels and 50% window overlap. The rotational flow (i.e. vorticity) field was determined by computing the mathematical curl of the measured velocity field. Localized concentrations of vorticity indicated the geometry of the vortex wake (Gharib et al., 1998) created by each animal during swimming (Figs 2 and 3; see also supplementary material Movies 1–7).

Wake kinetic energy measurement

The wake kinetic energy at the end of each swimming contraction was computed at each node i of the velocity field according to the definition $KE_i=1/2\rho\Delta V_i||\mathbf{u}_i||^2$, where ρ is the water density ($10^3\,kg\,m^{-3}$); ΔV_i is the volume of the node per unit depth and is equal to the product of the horizontal and vertical spacing of the velocity field grid, $\Delta x\Delta y$; and $||\mathbf{u}_i||$ is the magnitude of the velocity (i.e. the speed) at each node. To compute the mass-specific wake kinetic energy, the sum of the kinetic energy at all of the nodes in the vortex wake was divided by the cube of the bell diameter (although the mass of each animal was not directly measured, the density of each animal is approximately equal to the water density). The lateral and streamwise boundaries of the wake were defined as the edge of the region of vorticity created during each swimming cycle in which vorticity exceeded 20% of the maximum vorticity magnitude (cf. Fig. 3). This boundary was determined by manually outlining the vorticity contours in each frame using a custom MATLAB algorithm. The bell diameter was used as the characteristic length scale for each animal (*versus* bell height) in order to better capture the dependence on the size of the subumbrellar region where vortices are formed.

The calculations of kinetic energy used in the analyses are given per unit depth. For 'top-hat' wake velocity profiles, the mean wake

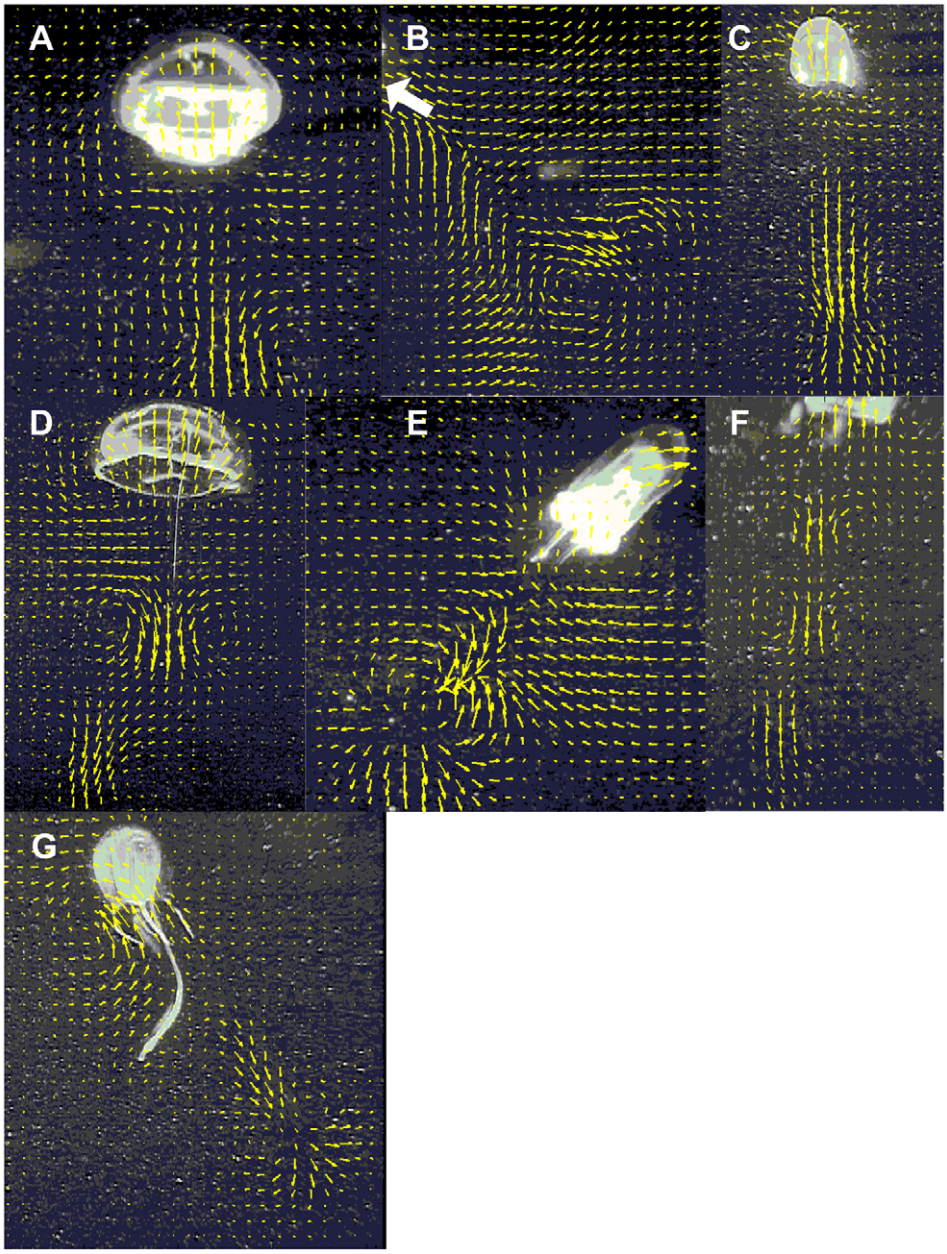

Fig. 2. Instantaneous velocity fields measured using digital particle image velocimetry (DPIV). (A) *Aeqorea*, (B) *Leuckartiara*, (C) *Melicertum*, (D) *Mitrocoma*, (E) *Neoturris*, (F) *Phialidium*, (G) *Sarsia* sp. White arrow in B indicates the position of the animal. Vectors are of order 1 cm s^{-1}. Bell diameters are indicated in Fig. 1.

velocity calculated in this way is identical to the result from an alternative axisymmetric wake assumption. For parabolic wake velocity profiles, the axisymmetric mean wake velocity is 25% less than the mean velocity calculated per unit depth (Smits, 2000). Starting vortical flows, such as those of the jellyfish, will be intermediate between the 'top-hat' and parabolic profiles (Didden, 1979), so we expect the error in the mean wake velocity to fall between these two extremes. This bias error was deemed preferable to the large, random errors introduced by the alternative assumption of axisymmetry, which is only approximately satisfied by the animal body and which rapidly breaks down in the wake. The relative comparisons between the species – the primary objective of this study – are unaffected by the consistent bias error and associated measurement uncertainty.

We took care to ensure that the normalizations based on bell diameter did not create artificial trends among the animals. For example, we verified that there is indeed no correlation between the normalized wake kinetic energy and the bell diameter. The species with largest and smallest normalized wake kinetic energy (*Leuckartiara* sp. and *Phialidium* sp., respectively) possess the two intermediate bell diameters.

Since the measurements of wake kinetic energy were made subsequent to the formation of the wake vortices, there is the potential for kinetic energy dissipation in the wake prior to each measurement. In principle, the wake vortices can break down into smaller eddies *via* inviscid mechanisms on times scales of d/u, where d is the vortex size and u is the vortex velocity (Tennekes and Lumley, 1972). However, this process is suppressed at the relatively low Reynolds numbers of the flows studied here (Rosenhead, 1963; Saffman, 1978). Indeed we did not observe any cascading of the wake vortices to smaller eddies on time scales shorter than the individual swimming cycles, which were themselves longer than d/u.

In the absence of inviscid breakdown of the wake vortices, viscous dissipation by interaction of opposite-signed vorticity remains the only mechanism available to dissipate kinetic energy. The relevant

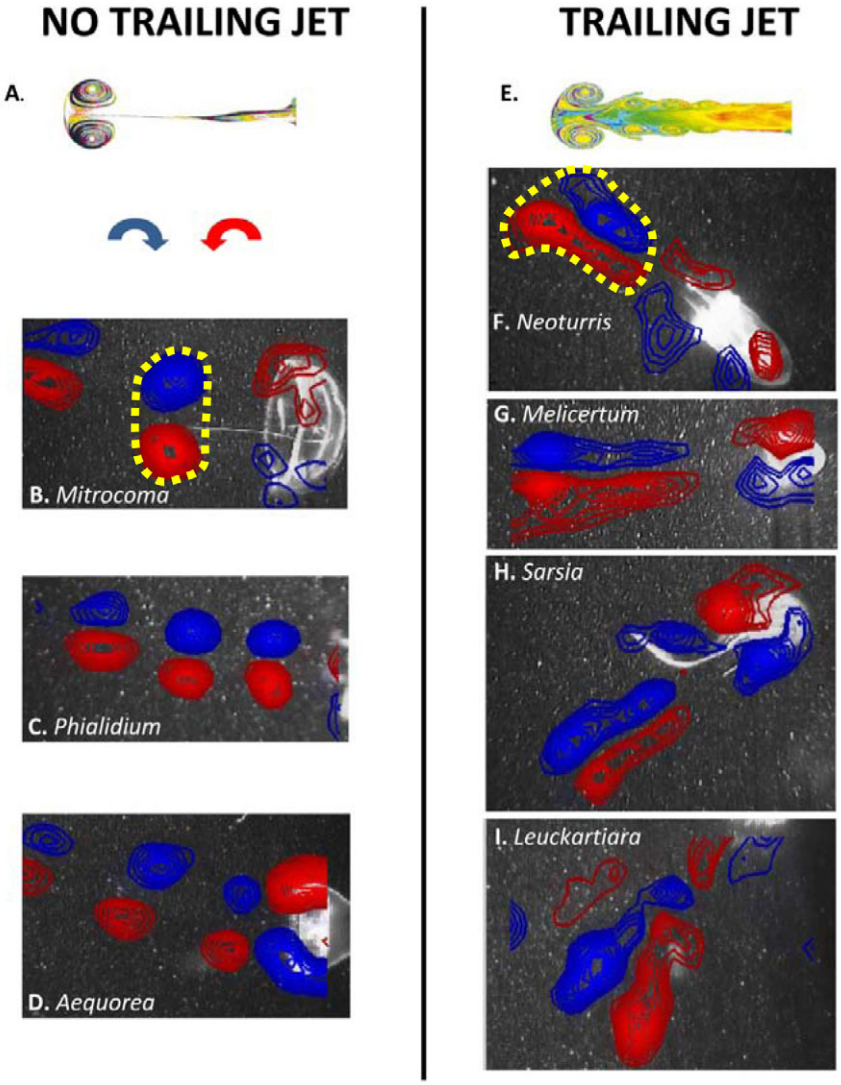

Fig. 3. Vortex wake classifications. Left panel, vortex wakes exhibiting no trailing jet formation. (A) Laser-induced fluorescence dye visualization of vortex ring formation without a trailing jet in a simplified mechanical vortex ring generator (Gharib et al., 1998), (B–D) Vorticity fields computed from DPIV measurements of free-swimming *Mitrocoma*, *Phialidium* and *Aequorea*, respectively. Blue and red contours denote clockwise and anticlockwise fluid rotation, respectively. Contours identify vorticity above 20% of the maximum vorticity in the wake. Yellow dashed curves illustrate regions defined as the wake for subsequent kinetic energy measurements. Right panel, vortex wakes exhibiting trailing jet formation. (E) Laser-induced fluorescence dye visualization of vortex ring formation with trailing jet in a simplified mechanical vortex ring generator (Gharib et al., 1998). (F–I) Vorticity fields computed from DPIV measurements of free-swimming *Neoturris*, *Melicertum*, *Sarsia* and *Leuckartiara*, respectively. See also supplementary material Movies 1–7.

time scale can be deduced from dimensional analysis given the known units of kinematic viscosity ν and the vortex length scale d (i.e. $cm^2\,s^{-1}$ and cm, respectively), which are the relevant parameters for the viscous dissipation (Rosenhead, 1963):

$$\tau = \frac{d^2}{\nu} . \quad (1)$$

For the typical eddy size (>0.25 cm) and kinematic viscosity ($10^{-2}\,cm^2\,s^{-1}$) of these experiments, the dissipation time scale τ>6 s, was significantly longer than the duration of bell contraction, which was typically around 300 ms and always less than 1 s. Therefore the viscous dissipation of wake kinetic energy that occurs prior to each measurement is assumed to be negligible.

Swimming proficiency measurement

The proficiency of swimming was quantified as the diameter-normalized swimming speed, U/D. The swimming speed was measured from the recorded sequences of swimming in the plane of the laser sheet, and was tracked based on the instantaneous position of the bell apex in each frame. In cases where the bell apex left the field of view during a swimming sequence, an alternate focal point on the body, e.g. the manubrium, was tracked in each frame. Intraspecific behavioral variations in swimming speed were reflected in the standard deviation of measurements within species.

Froude efficiency measurement

The propulsive efficiency provides a combined measure of wake energy expenditure and swimming proficiency and can be expressed as the dimensionless Froude efficiency η:

$$\eta = \frac{F_{drag}U}{F_{drag}U + P_{loss}} , \quad (2)$$

where F_{drag} is the hydrodynamic drag, U is the swimming speed, and P_{loss} is the flux of kinetic energy into the wake per unit time.

The hydrodynamic drag (F_{drag}) on each animal was estimated using an empirical drag coefficient model for streamlined bodies (Hoerner, 1965):

$$C_D = 0.003\,(1 + 1.5\,(D/H)^{3/2} + 7\,(D/H)^3), \quad (3)$$

where D is the bell diameter, H is the bell height, and the drag coefficient is based on wetted area.

The relatively low drag coefficients predicted by this model, compared to a bluff body of similar shape and Reynolds number as the animals, are consistent with the reduction in form drag that occurs as a result of the downstream jet that forms at the rear of the animal body and merges with the ambient flow around the body. Moreover, since this is a comparative study, our primary concern is to use a consistent drag model throughout. Other drag models may affect the

absolute value of the drag for each species but should not appreciably alter their relative values.

The power loss (P_{loss}) is due to the kinetic energy flux into the wake, and was calculated by dividing the measured wake kinetic energy by the duration of the ejection phase of the swimming cycle. Since the kinetic energy was calculated per unit depth, the drag force was also normalized per unit depth so that the Froude efficiency is dimensionless.

Statistical analysis of interspecific wake differences

Analysis of variance (ANOVA, Statistica, StatSoft Inc.) was used to test the significance of interspecific variations in wake characteristics. Raw data were log transformed to satisfy the homogeneity of variances assumption inherent to ANOVA. Interspecific variation dominated the overall variation in wake measurements and was highly significant (ANOVA, $P<0.0001$ for each of the variables, i.e. wake kinetic energy, proficiency and efficiency). Comparisons between particular species utilized contrast analysis within the ANOVA design. The wake traits of individual species and probability values of interspecific comparisons are listed in supplementary material Tables S1 and S2.

RESULTS

Fig. 2 shows representative measurements of the instantaneous velocity field created by each of the species. The wake structure is more clearly observable in the vorticity fields shown in Fig. 3.

We consistently observed two distinct wake patterns among the seven species studied. The first pattern consisted of isolated, radially symmetrical vortex rings, one created in the wake per swimming cycle (e.g. Fig. 3A–D). This wake pattern was shared by the species known to forage as cruising predators. The second pattern, observed for the species that forage as ambush predators, consisted of a vortex ring immediately followed by a trailing jet of water created during each swimming cycle (e.g. Fig. 3E–I).

Trailing jet formation is predicted to incur a higher energetic cost than the formation of multiple, isolated vortex rings of equivalent total fluid volume, and it is also predicted to manifest itself as higher kinetic energy content in the wake (Krueger and Gharib, 2003). To test these predictions we measured the wake kinetic energy of each species using the velocity field data. Fig. 4A shows that, on a mass-specific basis, those species forming trailing jets behind the vortex rings do indeed generate a higher flux of kinetic energy into the wake than species that do not form trailing jets. For this added cost, species that create trailing jets achieve more proficient locomotion, as measured by the normalized swimming speed (in body diameters per second; Fig. 4B).

Species forming trailing jets in the wake (cf. Fig. 3, right panel) exhibited relatively low propulsive efficiencies (Fig. 5). This is consistent with accepted notions of jet propulsion in animals as a low-efficiency mode of locomotion (Vogel, 1994; Anderson and Grosenbaugh, 2005), and confirms previous studies of mechanical vortex ring generators (Krueger and Gharib, 2003). By contrast, species forming discrete vortex rings without trailing jets (cf. Fig. 3, left panel) exhibited efficiencies exceeding 50%, significantly higher than the species that form trailing jets and comparable with the swimming efficiency of eels, for example (Kern and Koumoutsakos, 2006).

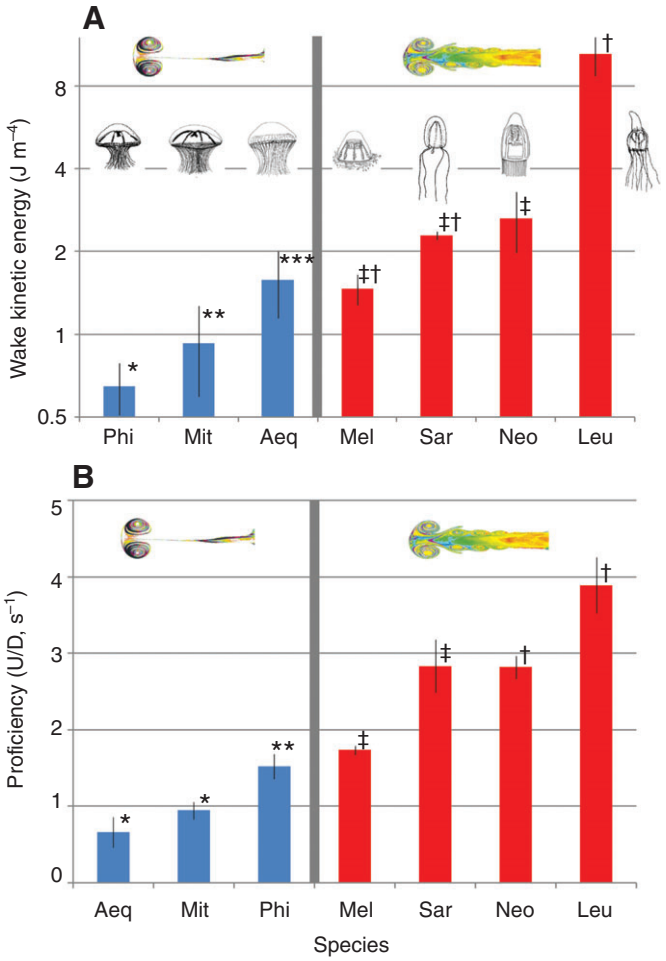

Fig. 4. (A) Wake kinetic energy measurements of each of the seven hydrozoan jellyfish species. Measurements are mass-specific for interspecific comparison. The standard error of each measurement is indicated by a vertical bar. Single asterisk, statistically significant difference from *Melicertum* (Mel), *Sarsia* (Sar), *Neoturris* (Neo) and *Leuckartiara* (Leu; see supplementary material Tables S1 and S2 for *P*-values and sample sizes, respectively). Double asterisk, statistically significant difference from *Neoturris* and *Leuckartiara* (contrast analysis within ANOVA; $P<0.05$). Triple asterisk, statistically significant difference from *Leuckartiara*. Single dagger, statistically significant difference from *Phialidium* (Phi), *Mitrocoma* (Mit) and *Aequorea* (Aeq). Double dagger, statistically significant difference from *Phialidium* and *Mitrocoma*. Triple dagger, statistically significant difference from *Phialidium*. Inset: images representing the two corresponding wake vortex motifs (adapted from Gharib et al., 1998). (B) Swimming proficiency measurements of each of the seven hydrozoan jellyfish species. Standard error of each measurement is indicated by a vertical bar. Single asterisk, statistically significant difference from *Melicertum*, *Neoturris*, *Sarsia* and *Leuckartiara* (see supplementary material Tables S1 and S2 for *P*-values and sample sizes, respectively). Double asterisk, statistically significant difference from *Neoturris* and *Leuckartiara*. Single dagger, statistically significant difference from *Aequorea*, *Mitrocoma* and *Phialidium*. Double dagger, statistically significant difference from *Aequorea* and *Mitrocoma*. Inset: images representing the two corresponding wake vortex motifs (adapted from Gharib et al., 1998).

DISCUSSION

These measurements provide the first confirmation that not only is the physical theory of optimal vortex formation directly reflected in the wakes of swimming animals (cf. Bartol et al., 2008; Bartol et al., 2009; Dabiri, 2009), but that the contrasting wake patterns on either side of the optimal vortex formation threshold (i.e. trailing jet *versus* no trailing jet) represent propulsive correlates to the ecological requirements of the different foraging modes.

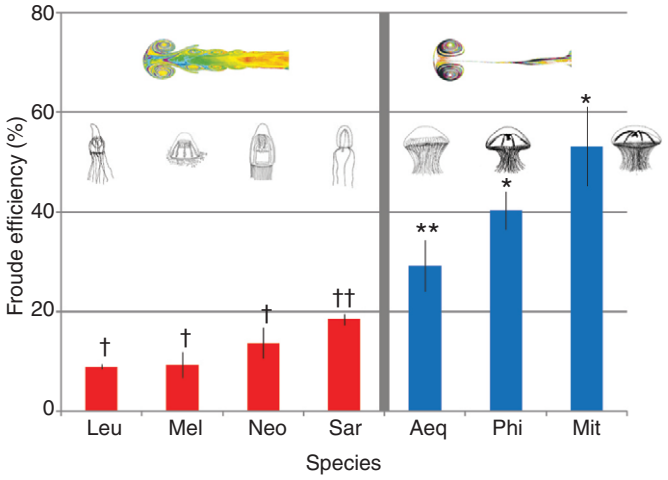

Fig. 5. Froude efficiency measurements of each of the seven hydrozoan jellyfish species. The standard error of each measurement is indicated by a vertical bar. Single dagger, statistically significant difference from *Aequorea* (Aeq), *Phialidium* (Phi) and *Mitrocoma* (Mit; contrast analysis within ANOVA; $P<0.05$; see supplementary material Tables S1 and S2 for *P*-values and sample sizes, respectively). Double dagger, statistically significant difference from *Phialidium* and *Mitrocoma*. Single asterisk, statistically significant difference from *Leuckartiara* (Leu), *Melicertum* (Mel), *Neoturris* (Neo) and *Sarsia* (Sar). Double asterisk, statistically significant difference from *Leuckartiara*, *Melicertum* and *Neoturris*. Inset: images representing the two corresponding wake vortex motifs.

This relationship might be expected if results from previous theoretical and experimental studies using simple mechanical vortex ring systems were certain to be applicable to living swimmers and fliers. However, direct confirmation has been limited by the lack of suitable approaches to test these hypotheses with freely moving, living organisms. It is important to emphasize that this relationship between physical theory and functional ecology transcends simple phylogenetic boundaries within medusan jellyfish lineages. For example, the Leptomedusae contain species that produce vortex wakes both with (e.g. *Melicertum* sp.) and without (e.g. *Aequorea victoria*, *Phialidium gregarium*, *Mitrocoma cellularia*) trailing jets (Fig. 6).

An examination of the relationship between efficiency and proficiency among the species examined (Fig. 7) clearly demonstrates the trade-offs associated with different propulsive and foraging strategies among medusae. The species that forage by continuously cruising (Colin et al., 2003) create discrete vortex rings without trailing jets. These cruising species exhibit low swimming proficiency – they swim slowly – but their swimming efficiencies are relatively high and depend on additional factors such as the wake vortex ring spacing (Weihs, 1977). Conversely, the ambush foraging species (Colin et al., 2003) create wake vortex rings with trailing jets. These ambush foragers are comparatively inefficient energetically, but their swimming proficiencies are relatively high and depend on additional factors such as body shape (Hoerner, 1965; Daniel, 1983). Among the jellyfish studied here, there exists a void in performance space where no animals can swim both efficiently and proficiently. This may be a consequence of the limited muscular capacity of jellyfish, a limit that has previously been shown to dictate the overall range of possible jellyfish morphologies and sizes (Costello et al., 2008). However, one species, *Melicertum*, did not appear to swim either efficiently or proficiently. Based on its wake structure and bell morphology (i.e. high fineness ratio) it swims using jet propulsion similar to the other ambush species (Colin and Costello, 2002). *Melicertum* is unique in that it is the only leptomedusa that we have examined which uses jet propulsion. Previously examined leptomedusae swim by what has been termed rowing propulsion (Colin and Costello, 2002). Unfortunately few details are currently known about the foraging behavior of *Melicertum*, limiting our ability to better relate its swimming to its foraging in this study.

The performance and energetic characteristics we have identified are consistent with the ecological needs of the different foraging strategies. Species that forage as cruising predators create more energy-efficient wakes, enabling them to swim for long durations with low energy expenditure, albeit at moderate speeds because of their associated lower swimming proficiency (Fig. 4B). Swimming efficiency is critical for these predators, which swim for more than 80% of the time (Colin et al., 2003) in order to entrain and transport fluid past their capture surfaces. However, since swimming by cruising–foraging jellyfish is used to create a feeding current, proficiency (i.e. swimming speed) is not as critical as entraining large volumes of fluid with each pulse.

Conversely, wake analysis demonstrates that ambush foraging species swim more proficiently but at higher energetic cost. However, ambush foraging jellyfish rarely swim in nature (<30% of the time), drifting motionlessly with their tentacles extended and waiting for prey to swim into their capture surfaces. Consequently, swimming is only used to escape predation and reposition themselves in the water column (Colin et al., 2003). Swimming proficiency is a necessity to avoid predators and to minimize the time between feeding bouts while repositioning, and energetic efficiency is a secondary requirement for survival. Together, these results provide a mechanistic connection between animal–fluid interactions and the functional ecology of jellyfish. The dichotomy between foraging modes that is predicted by the wake vortex structure is clearly observed in the species reported here and reflects broader patterns among medusan jellyfish lineages (Costello et al., 2008).

Although our data indicate that adults within a species cannot simultaneously maximize both swimming proficiency and efficiency, the morphological and behavioral bases of swimming may be plastic enough to allow different developmental stages to maximize different swimming modes. For example, recent evidence indicates that developmental alterations in morphology allow some Leptomedusae to transition away from trailing jet formation during their life cycle (Weston et al., 2009). Likewise, squid ontogeny involves transitions between stages with and without trailing jets in the vortex wake (Bartol et al., 2008). In the case of adult squid, the recruitment of lateral fins at low speeds appears concomitant with the cessation of trailing jet formation. Similar to the behavioral consequences observed in jellyfish, the low-speed swimming (i.e. without trailing jet formation) is known to be less energetically costly than the high-speed swimming (i.e. with trailing jet formation), which is used to escape predation (Anderson and Grosenbaugh, 2005; Bartol et al., 2008). These patterns indicate that developmental alterations in wake structures may be valuable indicators of life stage-dependent variations in selective forces affecting species survival.

Additional analogies to the dichotomy observed in the jellyfish may also be found in insect flight. Whereas most insects hover with wings beating in a horizontal plane for efficient propulsion, some species, which are more adept at achieving high accelerations, beat their wings in a nearly vertical plane (Ennos,

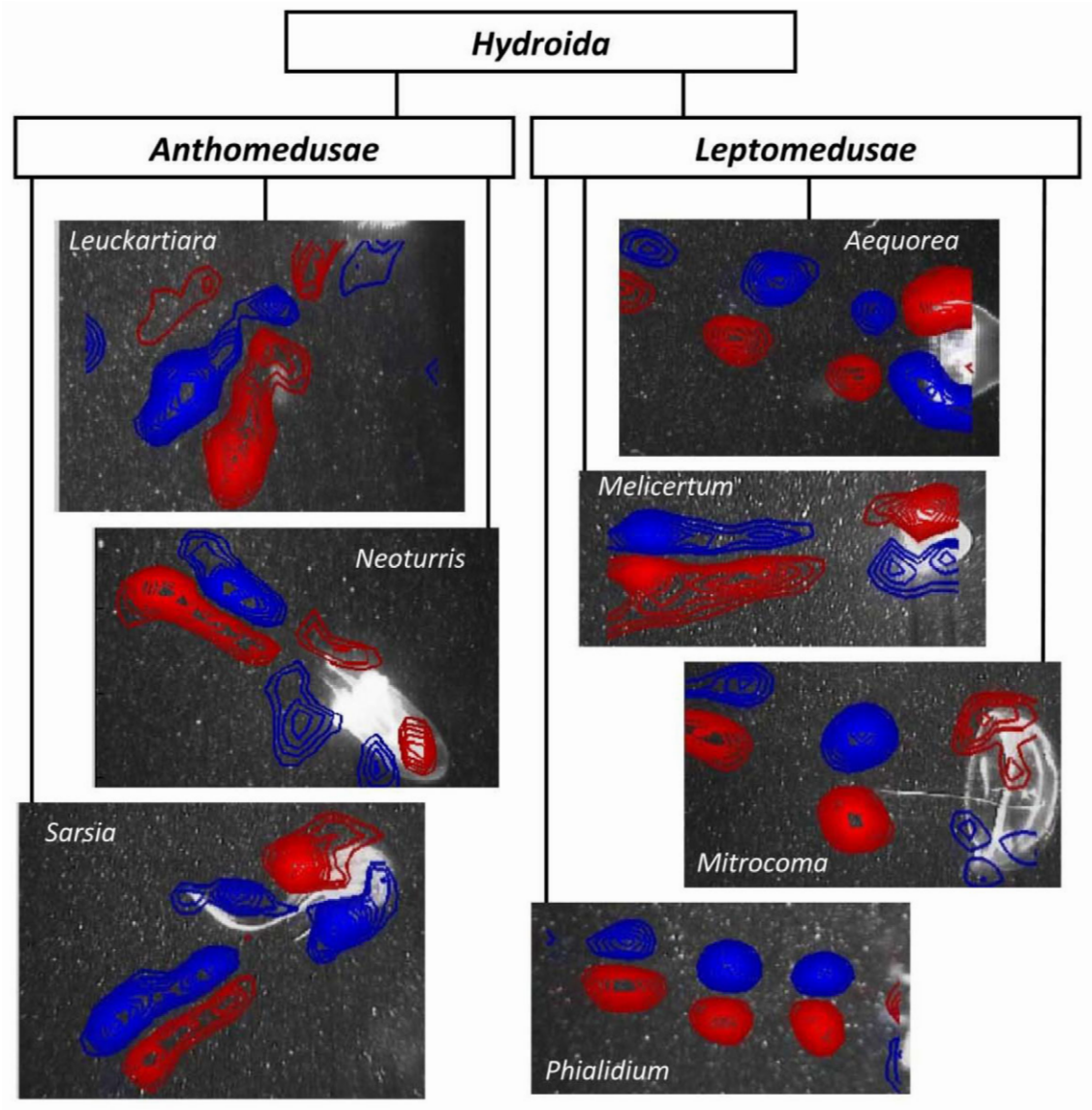

Fig. 6. Systematic relationships of co-occurring jellyfish species studied. Line length does not indicate relatedness.

1989; Dudley, 2000). The wake structures generated by these two modes of locomotion may reflect similar trade-offs to those observed in the present study.

The utility of the optimal vortex formation concept for biological locomotion lies in its generality. Although the theoretical analysis of Benjamin (Benjamin, 1976), which demonstrates the existence of an energetic constraint on vortex ring growth, is strictly valid for circular vortex rings, empirical evidence suggests that the process is manifested in a variety of more complex wakes consisting of non-circular vortex loops and chains (Dabiri, 2009). These include flows created by flapping plates in the range of Reynolds numbers that is relevant to lift- and drag-based swimming and flying (Milano and Gharib, 2005; Ringuette et al., 2007). Therefore, we expect that the experimental methods and wake energy analysis developed here can be directly applied to study animal–fluid interactions in higher aquatic and aerial organisms. In many of these animals, the occurrence of optimal vortex formation has already been hypothesized to occur (Linden and Turner, 2004; Milano and Gharib, 2005; Dabiri, 2009). However, since the vortex wakes consist of more complex loop and chain arrangements (Drucker and Lauder, 1999; Hedenstrom et al., 2007), the analyses may require three-dimensional flow velocimetry or numerical simulations in addition to the underlying physical approaches described here.

A note on three-dimensional data reconstruction

Since the measurements in this study are strictly two-dimensional, it is useful to consider the uncertainty introduced in three-dimensional reconstructions of the data that might be pursued to combine these results with studies of other swimming and flying animals. As described in the Materials and methods, the wake kinetic energy is calculated from the DPIV measurements as:

$$KE = \sum_{i=1}^{N} KE_{\mathrm{i}} = \frac{1}{2}\rho \sum_{i=1}^{N} \Delta V_{\mathrm{i}} \left\| \mathbf{u}_{\mathrm{i}} \right\|^2 , \quad (4)$$

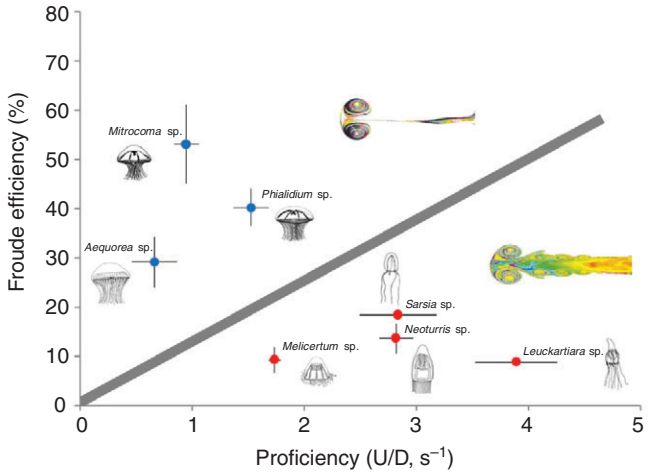

Fig. 7. Swimming efficiency *versus* proficiency of each of the seven hydrozoan jellyfish. Standard error of the measurements is indicated by black bars. Inset: images representing the two corresponding wake vortex motifs (adapted from Gharib et al., 1998).

where N is the number of nodes in the wake. The measurement uncertainty ε_{KE_i} (in joules) at each node is given by (Kline and McClintock, 1953):

$$\varepsilon_{KE_i} = \sqrt{\left(\frac{\partial KE_i}{\partial \Delta V_i}\varepsilon_{\Delta V_i}\right)^2 + \left(\frac{\partial KE}{\partial \left\|\mathbf{u}_i\right\|}\varepsilon_{\left\|\mathbf{u}_i\right\|}\right)^2} = \frac{1}{2}\rho\sqrt{\left(\left\|\mathbf{u}_i\right\|^2 \varepsilon_{\Delta V_i}\right)^2 + \left(2\Delta V_i \left\|\mathbf{u}_i\right\| \varepsilon_{\left\|\mathbf{u}_i\right\|}\right)^2}\ , \quad (5)$$

where $\varepsilon_{\Delta V_i}$ and $\varepsilon_{\|\mathbf{u}_i\|}$ are the uncertainties in the volume of node i and average flow velocity at node i, respectively. The fractional measurement uncertainty (in per cent/100) is therefore given by:

$$\frac{\varepsilon_{KE_i}}{KE_i} = \sqrt{\left(\frac{\varepsilon_{\Delta V_i}}{\Delta V_i}\right)^2 + \left(\frac{2\varepsilon_{\left\|\mathbf{u}_i\right\|}}{\left\|\mathbf{u}_i\right\|}\right)^2}\ . \quad (6)$$

Eqn 6 can be used to estimate the uncertainty that occurs when constructing a three-dimensional wake based on the two-dimensional DPIV measurements. As described in the Materials and methods, we estimate that the axisymmetric mean wake velocity is up to 25% less than the mean velocity calculated per unit depth. In Eqn 6, this corresponds to a value $\varepsilon_{\|\mathbf{u}_i\|}/\|\mathbf{u}_i\|=0.25$. The contribution to the total measurement uncertainty is therefore:

$$-0.5 < \left(\frac{2\varepsilon_{\left\|\mathbf{u}_i\right\|}}{\left\|\mathbf{u}_i\right\|}\right) < 0\ , \quad (7)$$

relative to the kinetic energy calculated per unit depth.

Whereas the node volume is assumed to be uniform across the wake in the per-unit-depth calculations, an axisymmetric calculation would result in the nodes further from the axis being of larger volume than those near the axis, since in each case the depth of the node is equal to the wake circumference at that position. If axisymmetry is assumed, the smallest node (at the body axis) has a volume:

$$\Delta V_{\min} \approx 2\pi\left(\frac{\Delta x}{2}\right)\Delta x \Delta y\ , \quad (8)$$

where $\Delta x/2$ is the average radius of the node and Δx and Δy are the transverse and streamwise node width, respectively. The largest node (at the radial extent of the wake) has a volume:

$$\Delta V_{\max} \approx 2\pi\left(\frac{D}{2}\right)\Delta x \Delta y\ , \quad (9)$$

where the average radius of the node is approximately equal to the radius of the animal. If one takes the median node volume as:

$$\Delta V_{\text{med}} = \frac{\Delta V_{\min} + \Delta V_{\max}}{2}\ , \quad (10)$$

then the maximum deviations from the median are:

$$\frac{\varepsilon_{\Delta V_{\min}}}{\Delta V_{\text{med}}} = \frac{2}{1 + D/\Delta x} - 1 \quad (11)$$

and

$$\frac{\varepsilon_{\Delta V_{\max}}}{\Delta V_{\text{med}}} = \frac{2}{1 + \Delta x/D} - 1\ . \quad (12)$$

For the present DPIV measurements, $0.08<\Delta x/D<0.2$. Therefore, the contribution to total measurement uncertainty is in the range:

$$-0.85 < \left(\frac{\varepsilon_{\Delta V_i}}{\Delta V_i}\right) < 0.85\ , \quad (13)$$

where both extremes correspond to $\Delta x/D=0.08$. In other words, the kinetic energy estimated per unit depth exhibits greatest deviation from axisymmetric calculations when the node width, Δx, is smallest relative to the wake diameter (i.e. cases with highest spatial resolution). The uncertainty is greatest at nodes located near the body axis and at the radial edge of the wake. Since the deviations are of opposite sign near the body axis and at the radial edge of the wake, their integrated effect in the calculation of total wake kinetic energy will be intermediate between these two extreme values (cf. intermediate value theorem).

The preceding analysis provides quantitative bounds on an equivalent axisymmetric flow constructed from the present two-dimensional DPIV measurements. Although such a construction is not essential for the qualitative comparisons in the present interspecific study, it may be needed in order to use the present measurement data in quantitative comparative studies of broader groups of swimming and flying animals. The relatively large uncertainty associated with three-dimensional reconstructions from the two-dimensional DPIV measurements suggests that quantitative comparisons between the present flow-based performance measurements (i.e. wake kinetic energy and Froude efficiency) and data from independent studies should be approached with caution and there is a need to remain mindful of the uncertainty bounds described in Eqns 7 and 13 when drawing conclusions.

ACKNOWLEDGEMENTS

The authors gratefully acknowledge helpful suggestions from the reviewers and funding from the National Science Foundation (OCE-0727587 and OCE-0623508 to J.H.C.; OCE-0351398 and OCE-0623534 to S.P.C.; OCE-0623475 to J.O.D.) and the Office of Naval Research (N000140810654 and N000140810918).

REFERENCES

Anderson, E. J. and Grosenbaugh, M. A. (2005). Jet flow in steadily swimming adult squid. *J. Exp. Biol.* **208**, 1125-1146.

Bartol, I. K., Krueger, P. S., Thompson, J. T. and Stewart, W. J. (2008). Swimming dynamics and propulsive efficiency of squids throughout ontogeny. *Int. Comp. Biol.* **48**, 720-733.

Bartol, I. K., Krueger, P. S., Stewart, W. J. and Thompson, J. T. (2009). Pulsed jet dynamics of squid hatchlings at intermediate Reynolds numbers. *J. Exp. Biol.* **212**, 1506-1518.
Benjamin, T. B. (1976). The alliance of practical and analytical insights into the non-linear problems of fluid mechanics. In *Applications of Methods of Functional Analysis to Problems in Mechanics* (ed. P. Germain and B. Nayroles), pp. 8-28. Berlin: Springer.
Bonner, J. T. (1965). *Size and Cycle: An Essay on the Structure of Biology*. Princeton: Princeton University Press.
Bouillon, J. and Boero, F. (2000). The hydrozoa: a new classification in the light of old knowledge. *Thalassia Salentina* **24**, 1-296.
Colin, S. P. and Costello, J. H. (2002). Morphology, swimming performance, and propulsive mode of six co-occurring hydromedusae. *J. Exp. Biol.* **205**, 427-437.
Colin, S. P., Costello, J. H. and Klos, E. (2003). *In situ* swimming and feeding behavior of eight co-occurring hydromedusae. *Mar. Ecol. Prog. Ser.* **253**, 305-309.
Collins, A. G., Schuchert, P., Marques, A. C., Jankowski, T., Medina, M. and Schierwater, B. (2006). Medusozoan phylogeny and character evolution clarified by new large and small subunit rDNA data and an assessment of the utility of phylogenetic mixture models. *Syst. Biol.* **55**, 97-115.
Costello, J. H., Colin, S. P. and Dabiri, J. O. (2008). The medusan morphospace: phylogenetic constraints, biomechanical solutions and ecological consequences. *Inv. Biol.* **127**, 265-290.
Dabiri, J. O. (2009). Optimal vortex formation as a unifying principle in biological propulsion. *Annu. Rev. Fluid Mech.* **41**, 17-33.
Dabiri, J. O., Colin, S. P., Costello, J. H. and Gharib, M. (2005). Flow patterns generated by oblate medusan jellyfish: field measurements and laboratory analyses. *J. Exp. Biol.* **208**, 1257-1265.
Daniel, T. L. (1983). Mechanics and energetics of medusan jet propulsion. *Can. J. Zool.* **61**, 1406-1420.
Didden, N. (1979). Formation of vortex rings – rolling-up and production of circulation. *Z. Angew. Math. Phys.* **30**, 101-116.
Drucker, E. G. and Lauder, G. V. (1999). Locomotor forces on a swimming fish: three-dimensional vortex wake dynamics quantified using digital particle image velocimetry. *J. Exp. Biol.* **202**, 2393-2412.
Dudley, R. (2000). *The Biomechanics of Insect Flight: Form, Function, and Evolution*. Princeton: Princeton University Press.
Ennos, A. R. (1989). The kinematics and aerodynamics of the free flight of some Diptera. *J. Exp. Biol.* **142**, 49-85.
Fish, F. And Lauder, G. V. (2006). Passive and active flow control by swimming fishes and mammals. *Annu. Rev. Fluid Mech.* **38**, 193-224.
Gharib, M., Rambod, E. and Shariff, K. (1998). A universal time scale for vortex ring formation. *J. Fluid Mech.* **360**, 121-140.
Hedenstrom, A., Johansson, L. C., Wolf, M., von Busse, R., Winter, Y. and Spedding, G. R. (2007). Bat flight generates complex aerodynamic tracks. *Science* **316**, 894-897.
Hoerner, S. F. (1965). *Fluid-Dynamic Drag*. Bakersfield: Hoerner Fluid Dynamics.
Kern, S. and Koumoutsakos, P. (2006). Simulations of optimized anguilliform swimming. *J. Exp. Biol.* **209**, 4841-4857.
Kline, S. J. and McClintock, F. A. (1953). Describing uncertainties in single-sample experiments. *Mech. Eng.* **75**, 3-8.
Kramp, P. L. (1959). The Hydromedusae of the Atlantic Ocean and adjacent waters. *Dana Rep.* **46**, 1-283.
Krueger, P. S. and Gharib, M. (2003). The significance of vortex ring formation to the impulse and thrust of a starting jet. *Phys. Fluids* **15**, 1271-1281.
Lighthill, J. (1973). On the Weis-Fogh mechanism of lift generation. *J. Fluid Mech.* **60**, 1-17.
Lighthill, J. (1975). *Mathematical Biofluiddynamics*. Philadelphia: Society for Industrial and Applied Mathematics.
Linden, P. F. and Turner, J. S. (2001). The formation of 'optimal' vortex rings, and the efficiency of propulsion devices. *J. Fluid Mech.* **427**, 61-72.
Linden, P. F. and Turner, J. S. (2004). 'Optimal' vortex rings and aquatic propulsion mechanisms *Proc. R Soc. Lond. B, Biol. Sci.* **271**, 647-653.
Marques, A. C. and Collins, A. G. (2004). Cladistic analysis of Medusozoa and cnidarian evolution. *Invert. Biol.* **123**, 23-42.
Milano, M. and Gharib, M. (2005). Uncovering the physics of flapping flat plates with artificial evolution. *J. Fluid Mech.* **534**, 403-409.
Mohseni, K., Ran, H. Y. and Colonius, T. (2001). Numerical experiments on vortex ring formation. *J. Fluid Mech.* **430**, 267-282.
Murray, C. D. (1926). The physiological principle of minimum work applied to the angle of branching of arteries. *J. Gen. Physiol.* **9**, 835-841.
Rayner, J. M. V. (1979). Vortex theory of animal flight. *J. Exp. Biol.* **91**, 697-796.
Rosenhead, L. (1963). *Laminar Boundary Layers*. New York: Dover Publications.
Ringuette, M., Milano, M. and Gharib, M. (2007). Role of the tip vortex in the force generation of low aspect ratio, normal flat plates. *J. Fluid Mech.* **581**, 453-468.
Saffman, P. G. (1978). The number of waves on unstable vortex rings. *J. Fluid Mech.* **84**, 625-639.
Smits, A. J. (2000). *A Physical Introduction to Fluid Mechanics*. New York: John Wiley and Sons.
Tennekes, H. and Lumley, J. L. (1972). *A First Course in Turbulence*. Cambridge: MIT Press.
Thompson, D. W. (1942). *On Growth and Form*. Cambridge: Cambridge University Press.
Valentine, J. W. (2004). *On the Origin of Phyla*. Chicago: University of Chicago Press.
Valentine, J. W., Collins, A. G. and Meyer, C. P. (1994). Morphological complexity increase in metazoans. *Paleobiology* **20**, 131-142.
Vogel, S. (1994). *Life in Moving Fluids*. Princeton: Princeton University Press.
Weihs, D. (1977). Periodic jet propulsion of aquatic creatures. *Forts. Zool.* **24**, 171-175.
Weston, J., Colin, S. P., Costello, J. H. and Abbott, E. (2009). Changing form and function during development in rowing hydromedusae. *Mar. Ecol. Prog. Ser.* **374**, 127-134.
Willert, C. E. and Gharib, M. (1992). Digital particle image velocimtry. *Exp. Fluids* **10**, 181-193.